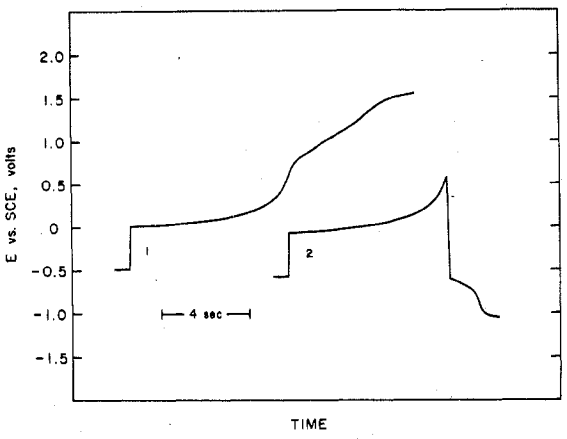

Figure 4. Anodic and current-reversal chronopotentiograms for 5.92×10^{-4} M $(CH_3)_4NB_3H_8$ in aqueous unbuffered 1 M potassium nitrate solution obtained with a gold wire electrode at room temperature; the current was 360 μA and the electrode area and radius were 0.355 cm^2 and 0.0318 cm, respectively.

lost with the resultant formation of the B_3H_7·DMF species. On the other hand, the B_3H_9 believed to be formed from protonation of $B_3H_8^-$ in dimethylformamide slowly reduces the solvent. Such is not the case in acetonitrile, for B_2H_6 (and, one would expect, B_3H_9) reacts with the solvent to form BH_3·$NCCH_3$ which slowly trimerizes to yield $(CH_3CH_2)_3N_3B_3H_3$.[16]

Studies in Water. Although the situation in water is believed to be similar to that encountered in dimethylformamide, the species involved are so much less stable that our conclusions are more tenuous. A chronopotentiogram for the oxidation of $B_3H_8^-$ at a gold anode in an unbuffered aqueous potassium nitrate medium exhibits three waves, as shown in Figure 4, curve 1. It is suggested that the first wave at +0.1 vs. SCE corresponds to the reaction

$$B_3H_8^- \xrightarrow{H_2O} B_3H_7{\cdot}OH_2 + {}^1/_2H_2 + e^- \quad (7)$$

because bubbles of hydrogen gas form at the surface of the anode. If the current is reversed at the transition time of the first wave for oxidation of $B_3H_8^-$ (Figure 4, curve 2), a cathodic wave appears at −0.7 V, signaling the reduction of hydrogen ion formed by oxidation of molecular hydrogen at the electrode surface during oxidation of $B_3H_8^-$.

Conceivably, the second, greatly attenuated wave at +0.85 V might arise from oxidation of B_3H_7·OH_2 to a hydrated form of BH_2^+. However, both of these species are exceedingly unstable in an aqueous solution, being rapidly converted to borates. Formation of a gold oxide film on the surface of the anode is responsible for the third wave at +1.1 V.

Controlled-potential coulometric oxidations of $B_3H_8^-$ at +0.5 and +1.0 V showed the transfer of at least 6 equiv/mol of $B_3H_8^-$. This result varied with the initial concentration of $B_3H_8^-$ and with the pH of the solution. Apparently, the H^+ produced by oxidation of the H_2 generated in reaction 7 reacts vigorously with $B_3H_8^-$ to form what can be visualized as an aqueous solution of diborane—a very unstable, highly reducing mixture.[17] Therefore, although it is unrealistic to attempt to reach quantitative conclusions from the coulometric data, it is clear that an oxidation of $B_3H_8^-$ takes place in an aqueous medium. However, because water is a protic solvent, sufficient complications occur to make further investigations unwarranted at this time.

Registry No. $(CH_3)_4NB_3H_8$, 12386-10-6; B_3H_7·$NCCH_3$, 59796-67-7; $(CH_3)_3N$·BH_3, 75-22-9; B_3H_7·DMF, 59803-46-2; $(C_2H_5)_3N$·BH_3, 1722-26-5; $(C_3H_7)_3N$·BH_3, 15201-50-0; $(C_4H_9)_3N$·BH_3, 2080-00-4; B_4H_{10}, 18283-93-7; acetonitrile, 75-05-8; dimethylformamide, 68-12-2; $(C_3H_7)_4NB_3H_8$, 59796-66-6; $(C_2H_5)_4NB_3H_8$, 12555-74-7.

References and Notes

(1) Taken in part from the Ph.D. theses of J. H. Kindsvater, 1972, and P. J. Dolan, 1974, Indiana University, Bloomington, Ind. Financial support from the National Science Foundation is gratefully acknowledged. Advice and assistance of David C. Moody and Nicholas C. Bensko with operation of the ^{11}B NMR spectrometers and the chronopotentiometric equipment is appreciated.
(2) J. A. Gardiner and J. W. Collat, *Inorg. Chem.*, **4**, 1208 (1965).
(3) R. L. Middaugh and F. Farha, *J. Am. Chem. Soc.*, **88**, 4147 (1966).
(4) R. J. Wiersema and R. L. Middaugh, *J. Am. Chem. Soc.*, **89**, 5078 (1967).
(5) J. Q. Chambers, A. D. Norman, M. R. Bickell, and S. H. Cadle, *J. Am. Chem. Soc.*, **90**, 6056 (1968).
(6) D. F. Shriver, "The Manipulation of Air-Sensitive Compounds", McGraw-Hill, New York, N.Y., 1969.
(7) D. F. Gaines, R. Schaeffer, and F. Tebbe, *Inorg. Chem.*, **2**, 526 (1963).
(8) J. J. Lingane, *J. Electroanal. Chem.*, **1**, 379 (1960).
(9) D. G. Peters and W. D. Shults, *J. Electroanal. Chem.*, **8**, 200 (1964).
(10) J. Vedel and B. Tremillon, *J. Electroanal. Chem.*, **1**, 241 (1959).
(11) L. W. Marple, *Anal. Chem.*, **39**, 844 (1969).
(12) C. E. Cutchens, M.S. Thesis, Indiana University, Bloomington, Ind., 1964.
(13) (a) D. G. Peters and J. J. Lingane, *J. Electroanal. Chem.*, **2**, 1 (1961); (b) D. G. Peters and A. Kinjo, *Anal. Chem.*, **41**, 1806 (1969).
(14) R. Schaeffer, F. Tebbe, and C. Phillips, *Inorg. Chem.*, **3**, 1475 (1964).
(15) J. H. Kindsvater, personal communication of unpublished results.
(16) H. J. Emeléus and K. Wade, *J. Chem. Soc.*, 2614 (1960).
(17) W. L. Jolly and T. Schmitt, *J. Am. Chem. Soc.*, **88**, 4282 (1966).

Contribution from the Union Carbide Corporation, Nuclear Division, Oak Ridge Y-12 Plant, Oak Ridge, Tennessee

The Kinetics of the Boron Plus Nitrogen Reaction

J. B. CONDON,* C. E. HOLCOMBE, D. H. JOHNSON, and L. M. STECKEL

Received March 1, 1976 AIC60156H

The reaction kinetics between boron and nitrogen have been examined in the temperature range of 1479 to 1823 K, using amorphous (probably α-phase) boron and β-rhombohedral boron. The evidence indicates the reaction mechanism is most likely topochemical yielding BN with α-B as the starting material. When β-B is the starting material, a two-step reaction series occurs with an homogeneous reaction to form B_6N followed by a topochemical reaction to yield BN.

Introduction

The direct boron–nitrogen reaction was selected to test the applicability of a proposed gas–solid reaction mechanism. Listed in Table I are some solid–diatomic gas reaction mechanisms encountered and their distinguishing kinetic features. These are the mechanisms that are operative for reactions going to completion. A topochemical mechanism is defined as a reaction that is rate limited by the process occurring at the interface between the product and a solid reactant. Thin-film mechanisms are not included. The mechanisms are listed in Table I as if only one reaction step were rate limiting. It is also possible to obtain a reaction with multiple rate-limiting steps that is not easily catalogued by these classifications. It was the original intent of the work reported here to test a reaction other than a metal–hydrogen reaction for applicability of the reactant-phase diffusion model.

Table I. Characteristics of the Three Basic Mechanisms for a Solid–Diatomic Gas Reaction

Characteristic	Product phase diffusion: Atomic diffusion	Product phase diffusion: Molecular diffusion	Topochemical (phase boundary movement)	Reactant phase diffusion–nucleation
Rate law with respect to solid: Massive pieces	Parabolic or paralinear law		Linear rate law	Variable
Rate law with respect to solid: Fine powder	Calculable from parabolic (see Appendix)		Nearly first order	First order
Rate law with respect to gas phase	Half order[a]	First order[a]	Half order	Half order
Dependence on size of particles of powder	Directly dependent		Dependent	Independent
Microstructure of product of partial reaction	Surface layer		Surface layer	Homogeneous distribution of product phase in reactant phase

[a] Possibly modified by a surface adsorption, i.e., Langmuir isotherm.

In contrast to the models where diffusion occurs through either a protective or penetrable layer, the reactant-phase diffusion model is seldom observed. In this latter model, diffusion of the gas phase atoms in the starting solid phase is rapid relative to the precipitation of the product phase. This model has been previously proposed to account for the kinetics of the uranium–hydrogen reaction.[1] Internal oxidation of copper and silver base alloys[2,3] are other examples, although these are somewhat complicated by the variety of product stoichiometries. As applied to pure reactants, the hydriding reaction appears to be the only known example.

To facilitate the study, the material was chosen on the basis of stability in air of both solid reactant and product. This allowed examination by x-ray diffraction, electron diffraction, and electron microscopy without extensive equipment modifications. Boron and boron nitride fulfill these requirements.

Another selection criterion was that the sample be "small enough" and the precipitation rate be "slow enough" in comparison to the diffusion coefficient. This allows complete diffusion throughout the sample before any appreciable reaction takes place. (This criterion has been calculated and reported.[4]) In the present case, a quick comparison of the diffusion of nitrogen in boron to the powder sizes and reaction rates reveals this combination to be a reasonable candidate for this mechanism. The direct combination of boron with nitrogen to form BN has been known for over a century and is generally observed to be very slow.[5] The recorded diffusion coefficient of nitrogen in boron is relatively fast. According to Samsonov[6] the diffusion coefficient, D, is given by

$$D = 2.03 \times 10^{-4} e^{-2000/T} \quad (1)$$

above 1573 K. Thus for a 5 μm powder the time constant for diffusion at 1673 K is $\sim$0.5 ms. This contrasts nicely with the several hour time constant for BN formation.

Experimental Section

The boron powder used in these experiments was supplied by Callery Chemical Co. It was obtained by the thermal decomposition reaction of boron hydrides. The mean particle size of the starting material was 0.137 μm as measured by photolometer (lower 10% $\leq$0.056 μm and upper 10% $\geq$0.222 μm). Excluding adsorbed water, the total impurity level was less than 610 ppm as measured by spark-source mass spectroscopy (the three highest impurities were Si = 150 ppm, Na = 60 ppm, and Cl = 40 ppm). The nitrogen used contained 50 vppm or less contamination excluding inert gas (100 vppm or less).

The kinetic studies were followed with the aid of a Mettler TGA system. The boron powder was contained in a crucible of BeO which was unreactive at the temperatures of interest. After admission of the sample to the balance, the balance chamber was evacuated to 1.3 $\times 10^{-3}$ Pa (10^{-5} Torr) or less. It was then backfilled with gettered argon for an anneal and the temperature was held constant for the prescribed time. The sample was then cooled and the chamber again evacuated. The temperature was again held constant under vacuum and a nitrogen flow established. Since the reaction was very slow, there was ample time for the balance to settle to a steady condition after admission of the nitrogen. Data were read after the balance had stabilized. Buoyancy and flow corrections were not made; therefore, the limiting stoichiometry calculated may be meaningless. However, the rate constants are correct.

Six sets of runs were performed. The nitriding step for the first three sets was run at 1 atm (0.101 MPa) of N_2 and differing temperatures from 1473 to 1773 K. In the first set, the annealing step was not included. The second and third set included annealing steps of 2 h at 1773 K and 1 h at 1873 K, respectively.

The fourth set included a series of annealing runs at 1873 K with times of 1, 2, 4, and 8 h. In this set, the nitriding was performed in 1 atm of N_2 at 1673 K. The pressure of N_2 was varied for the fifth series. The runs of this series were performed at 1673 K after 1-h 1873 K heat treatments. For the final series, the powder sample was annealed for 8 h at 1773 K in a separate furnace. This powder was subsequently fractionated by two different methods. One method was a separation from a settling bath of 3:1 ethanol–glycerol mix. The other method was micropore filtration using an acetone carrier liquid which passed through a 10-μm filter. Each collected fraction by both methods was reacted at 1673 K and 1 atm (0.101 MPa) of N_2 to determine if the rate correlated with surface area of the powder.

For each batch of starting material for nitriding, a particle-size determination was made using a Coulter counter. The Coulter counter was not used when the material was too fine for this measurement. This was the case for the unannealed material, where a photolometer was used to measure the particle size. Anneals identical with those performed before nitriding were made and particle size was determined on these similar samples rather than on the material used for reaction. The exception to this procedure was the sixth set where the powder was fractionated before nitriding, and there the particle size was determined from each batch used for the reaction.

The material used for electron microscopy and diffraction was taken from two special runs. These runs were at 1673 K and 1 atm (0.101 MPa) of N_2 after a 1-h 1873 K anneal. For one run, the reaction was stopped short at about 30% completion in order to inspect the morphology during the reaction. The other run was allowed to proceed to about 60% completion. These resultant powders were examined utilizing transmission electron microscopy (TEM) techniques. Portions of the powders were mounted in epoxy resin and sectioned by diamond knife ultramicrotomy. The powder reacted to 60% completion was also examined as a dispersion. This powder was ultrasonically dispersed in ethanol and dropped on a fenestrated carbon grid. Selected area electron diffraction (SAED) patterns and dark field (DF) microscopy were used to distinguish the various materials present and their orientations.

X-ray analysis was made of both starting material and product material for every run. Spark-source analyses were made for a few runs and oxygen analyses were performed for samples whose x-ray analyses showed large amounts of the phase designated B_6X, the pattern of which is very similar to B_6O (designated B_7O on Powder Diffraction File Card No. 12-614). The oxygen analysis of these samples did not exceed 1.1 wt %.

The rate constants were calculated by a linear least-squares analysis performed on the transformed equation. Although a nonlinear least-squares analysis is ordinarily in order for this type of determination, the accuracy of the experiment did not seem to warrant it.

Results

Kinetics. All reactions follow very closely the first-order kinetics in the remaining boron. The largest deviations from the first-order rate occurred immediately after the balance had

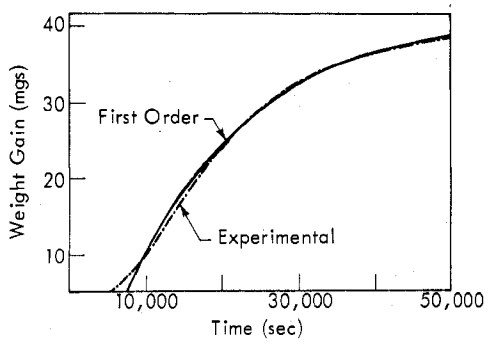

Figure 1. A comparison of the experimental weight gain curve of the B + N_2 reaction with the weight gain curve expected from a rate equation that is first order in remaining boron; that is rate $\propto$ (remaining boron).[1] This particular example is with nonheat-treated powder of median size of 0.137 μm reacted with 1 atm (0.101 MPa) of N_2 at 1483 K.

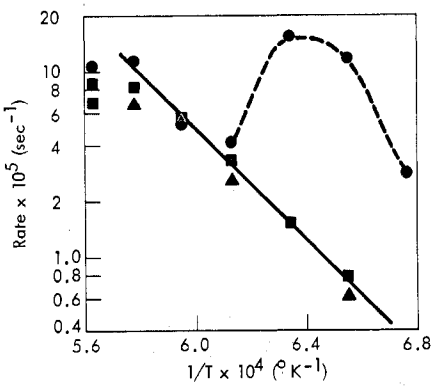

Figure 2. An Arrhenius plot of the rates of reaction of boron powders in 1 atm (0.101 MPa) of N_2. Points designated • are with as-received amorphous boron powder. Points designated ■ and ▲ used powders that were heat treated prior to reaction. These heat treatments were 1773 K for 2 h and 1873 K for 1 h, respectively.

settled from the nitrogen admission. This can be seen in a typical fit of the experimental data to a first-order rate in Figure 1. The fit to a product layer diffusion model was much worse (this fit would be similar to the first-order fit with time replaced by $(\text{time})^{1/2}$ as described in the Appendix). The first-order fit was typically within 1% with occasional deviations at the beginning of the reaction of up to 5%. However, the fit to a first-order rate does not distinguish between the reactant phase diffusion and topochemical mechanisms. This latter mechanism reflects a two-thirds order in the remaining solid reactant and is nearly identical to the first order. This two-thirds order rate law must be tested by an examination of the effects of the surface area as stated previously.[1]

The limiting stoichiometry, measured by weight gain, was typically around $BN_{0.6}$. This substoichiometry (to BN) was not all attributable to buoyancy and flow corrections. In fact, when the reaction was continued for several days after the sample had reached approximately 90% of extrapolated stoichiometry, the weight gain became linear albeit extremely slow. Thus, the first-order rate appears to apply only to the "fast" (time constant ~10 to 50 ks) initial reaction.

Figure 2 shows an Arrhenius plot of the first three sets of runs. At low temperatures (1473 to 1623 K) the nonheat-treated material reacted much more rapidly than the heat-treated material. To determine if this difference was due solely to particle size differences, the particle size of the heat-treated material (2 h at 1773 K) was determined by photolometer. This was necessary in order to make a comparison with the photolometer determination on the untreated sample. (Comparisons between Coulter counter method and the

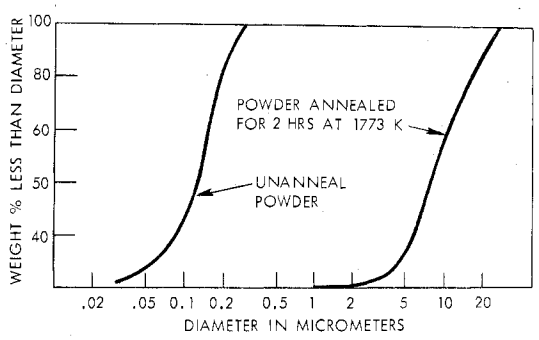

Figure 3. The particle size distribution for the nonheat-treated powder and the powder heat treated at 1773 K for 2 h. The ratio in size is approximately 60.

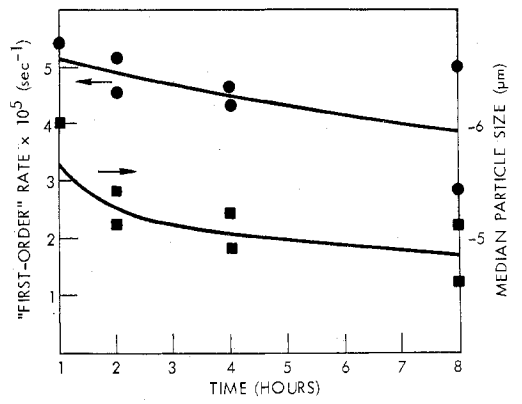

Figure 4. The observed "first-order" rates and particle size as a function of heat-treatment time. The reaction of the boron was at 1673 K in 1 atm (0.101 MPa) of N_2. There is an apparent negative correlation between reaction rate, shown as circles, and heat-treatment time. There is also either a slight negative or no correlation between particle size and heat treatment. These correlations would rule out the hypothesis that differences in rates are due solely to particle size differences.

photolometer may introduce a systematic error.) The distributions found are shown in Figure 3 (for untreated powder % <10 = 0.056 μm, % <50 = 0.137 μm, % <90 = 0.222 μm; for treated powder % <10 = 4.4 μm, % <50 = 8.8 μm, % <90 = 20.3 μm). The ratio in size is approximately 60 which would yield a rate difference of about a factor of 3600 for the mechanisms involving the two-thirds order law. For the topochemical mechanism, a "three-dimensional" particle (such as a sphere) will yield a two-thirds order law and a rate which is dependent on the inverse of the square of the radius. For "two-dimensional" particles such as rods, one obtains a one-third order law which is easily distinguished from the first-order law and a rate which is dependent on the inverse of the radius. Neither was observed.

An effective average activation energy of approximately 63 kcal is calculable from the slope of the solid line in Figure 2. This value probably has little significance, given the complexity of the reaction.

X-ray analysis of the starting material, however, revealed that the unannealed powder was amorphous, whereas the annealed material was β-rhomobohedral boron (or β-boron). Thus, a comparison of these rates reveals little about the reaction mechanism.

Correlations for the two anneal treatments (1 h at 1873 K and 2 h at 1773 K) between anneal temperature and the rate could not be made on the data used in Figure 2. The annealing treatment differed in both the time and temperature. The fourth set of runs was designed specifically to check the

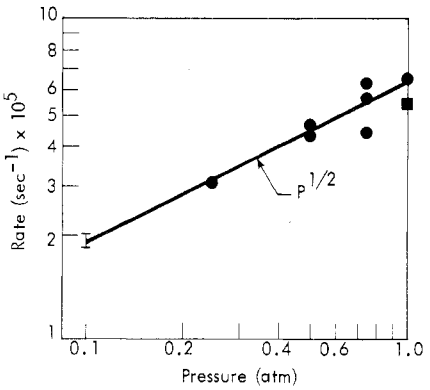

Figure 5. The dependence of the "first-order" reaction rate on the pressure of nitrogen. These reactions of heat-treated boron powder were performed at 1673 K. A reasonable fit is a half-power dependence of rate on nitrogen pressure. This is consistent with a mechanism whereby the rate-limiting step involves the dissociated form of nitrogen.

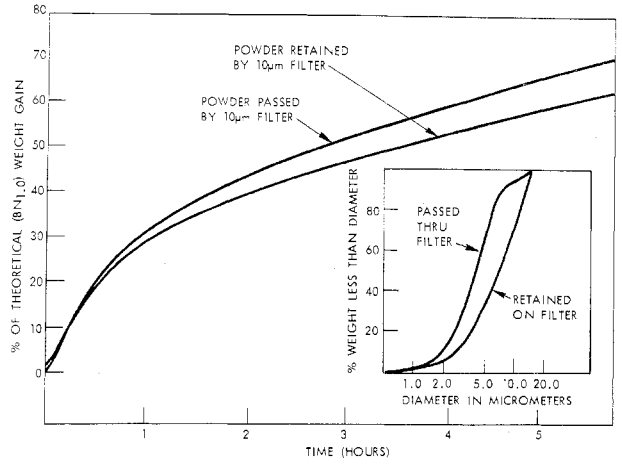

Figure 6. The relative weight gains as a function of reaction time for powder of two different size distributions. These powders came from the same heat treatment and were separated using a 10-μm filter. The two particle size distributions are compared in the lower right insert. A factor of ~2.5 difference would be expected in the rates if the pure topochemical mechanism applied.

correlation between the anneal treatment and the rate. Figure 4 gives the results of this set, and, with the exception of one data point, there is an inverse correlation between annealing time and the rate constant. However, there is no correlation made to particle size. (The proper dependence for a geometrically determined rate would have been inversely proportional to the square of the size.) The explanation for the correlation must again be attributed to the change in crystallinity of the powder.

To check the half-power dependence in nitrogen pressure, the fifth set of runs was made. Nitriding was carried out at 1673 K after a 1-h 1873 K anneal. The results of these runs are shown in Figure 5. The best choice for the dependence is indeed a half-power relation indicating atomic nitrogen is involved in the rate-limiting step.

The sixth set of runs was made to specifically determine if there was an effect of size on the rate. Table II shows the results of the runs made with the settling bath separated powders. Data are given in Figure 6 for the micropore separation, since a "first-order" rate equation fit poorly. In both cases, there is a correlation between the rate and particle size. The dependence, however, is not strong enough for a topochemical mechanism involving the two-thirds order law. It will be noted that when a linear rate constant is calculated (see Table II) an inverse correlation appears. Calculation of

Table II. Comparison of Reaction Rates Obtained from Two Different Particle Size Powders[a]

	Diameter, μm, with weights			"First order" rate constant, h^{-1}	Calculated linear[b] rate, nm h^{-1}
	<10%	<50%	<90%		
Upper	1.8	3.4	5.8	6.83×10^{-2}	31.6
Lower	2.2	4.2	7.2	6.12×10^{-2}	38.0

[a] Fractionation was accomplished by settling in a 3:1 ethanol-glycerol mixture. [b] The calculated linear rate is from the topochemical assumption using the particle size distribution found by Coulter counter and the method outlined in the Appendix.

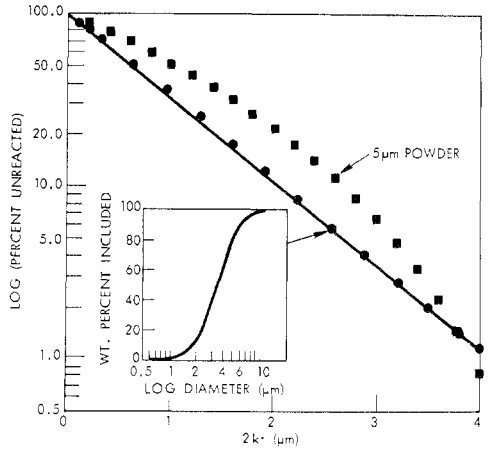

Figure 7. An illustration of how a distribution of particle sizes would make a pure topochemical mechanism ($^2/_3$ order with spherical particles) appear to follow an ideal first-order rate law. The squares are a calculation based on an ideally uniform 5 μm diameter spherical powder; whereas, the circles are a calculation based on a real particle size distribution shown in the insert (one of the powders in Table II). Calculation is explained in the Appendix.

the linear rate is obtained by using the particle size distribution and the method described in the Appendix. Results of this calculation on one of the fractions as compared to an idealized 5 μm diameter powder are shown in Figure 7. It can readily be seen that the distribution of particle sizes tends to make the rate appear more ideally "first order" in the remaining solid reactant. An insufficient dependence of rate on particle size was also observed for the micropore separated material. From its particle size distribution, one would expect a factor of ~2.5 between the rates of reaction for these two fractions. This does not occur.

X-Ray Analysis. The four species detected in this study by x-ray diffraction were amorphous material, β-boron, BN (usually distorted with expansion in C_0 parameter), and a species designated here as B_6X. This B_6X had an x-ray pattern similar to B_6O,[7] the generally accepted[8] stoichiometry for boron suboxide.

The starting material was found to be amorphous which other investigators[9-11] have indicated to be microcrystalline α-boron. The heat-treated starting material was β-boron with an occasional possible minor fraction of B_6X.

A summary of the x-ray results from the reacted material is given in Table III. The B_6X pattern was strongest for material that was preheat treated to convert the starting material to β-boron. Oxygen analyses on those materials in which B_6X was present as an intermediate were never greater than 1.1 wt % oxygen. This corresponds to the presence of ≤5.5 wt % B_6O assuming all the oxygen was present in the form of B_6O. A standard mixture of 5.5 wt % B_6O prepared by the reaction of ZnO and B[12] and 94.5 wt % BN indicated a minor fraction of B_6O in the x-ray diffraction analysis. Therefore, the B_6X material observed as an intermediate or

Table III. Summary of X-Ray Analysis for the Boron + Nitrogen Reaction

Pretreatment		Reaction conditions		X-ray analysis			% reacted (based on $BN_{1.0}$)		
Temp, K	Duration	Temp, K	N_2 pressure, atm	Majors	Intermediates	Minors[c]	Estimate from balance	Calcd extrapolation	"First-order" rate constant Ms^{-1}
1479[a]	15 min	1479	1	BN		(β-B)(B_6X)	~74	78.1	28.3
1528[a]	15 min	1538	1	BN	β-B	(B_6X)	~66	66	120
1578[a]	12 min	1578	1	BN	β-B	(B_6X)	~62	61.8	152
1629[a]	10 min	1629	1	BN		β-B (B_6X)	~72	75.7	41.5
1679[a]	15 min	1679	1	BN		(B_6X)	~75	82.9	52.2
1730[a]	12 min	1730	1	BN			~75	75.7	113
1777[a]	7.5 min	1777	1	BN			~73	77.6	106
1774	2 h	1478	1	β-B	BN		~8	*b*	*b*
1773	2 h	1522	1	BN	β-B	(B_6X)	~45	56.6	7.80
1773	2 h	1573	1	BN	β-B, B_6X		~56	67.4	14.6
1774	2 h	1626	1	BN	B_6X		~71	71.4	33.0
1774	2 h	1675	1	BN	B_6X		~65	72.9	55.3
1774	2 h	1723	1	BN		(B_6X)	~69	72.6	83.1
1773	2 h	1773	1	BN		B_6X	~75	79.3	67.7
1774	2 h + 20 min	1774	1	BN		(B_6X)	~71	75.5	85.6
1773 +1823[a]	2h 10 min	1823	1	BN		(B_6X)	~76	82.5	66.7
1873	1 h	1523	1	BN	β-B, B_6X		~43	55.0	6.15
1873	1 h	1623	1	BN	B_6X		~63	68.3	25.7
1873	1 h	1676	1	BN	B_6X		~60	65.9	54.2
1875	1 h	1723	1	BN	B_6X	β-B	~64	68.4	66.0
1873	1 h	1873	1	BN		B_6X	~71	83.3	65.0
1873	2 h	1673	1	BN	β-B, B_6X		~46	54.4	51.6
1873	4 h	1673	1	BN	β-B, B_6X		~38	48.3	46.4
1873	8 h	1673	1	BN, B_6X	β-B		~30	31.2	28.2
1873	2 h	1673	1	BN	B_6X		~57	62.4	45.2
1873	4 h	1673	1	BN	B_6X	β-B	~44	50.5	41.7
1873	8 h	1673	1	BN	B_6X	β-B	~36	38.8	49.9
1873	1 h	1675	0.75	BN	B_6X	β-B	~51	72.5	62.6
1873	1 h	1676	0.75	BN	B_6X	β-B	~60	65.0	56.3
1873	1 h	1675	0.75	BN	B_6X	β-B	~33	51.1	44.1
1873	1 h	1673	0.5	BN	B_6X	β-B	~53	58.2	43.2
1873	1 h	1673	0.5	BN	B_6X	(β-B)	~53	58.5	46.4
1873	1 h	1675	0.5	BN	B_6X	β-B	~42	52.8	39.0
1873	1 h	1670	0.25	BN, B_6X		β-B	~17	22.4	31.0
1873	1 h	1675	0.10	BN	B_6X	β-B	~18	29.3	19.4

[a] Not deliberate heat treated; isothermal condition established before N_2 admission. [b] Time of run too short to fit for rate. [c] Parentheses indicate "possibly"; i.e., the 100% peak is very faintly present.

major fraction in x-ray patterns must consist of more than just B_6O.

There appears to be a positive correlation between the presence of the B_6X and the combination of the higher reaction temperatures and more complete preconversion to β-boron. This statement assumes that the conversion to β-boron is more complete when the pretreatment temperature is higher and/or the treatment time is longer, as indicated by the electron diffraction and microscopy study by Runow.[13]

Morphology by Electron Microscopy. The 60% reacted powder that was ultrasonically dispersed consisted of chainlike agglomerates. These agglomerates were too thick to transmit electrons; therefore, SAED patterns were obtained only from the surface edges and asperities. The patterns obtained could always be indexed as BN (with an expanded C_0 parameter). A small number of whiskers were observed separate from the agglomerates. These whiskers were more transparent to the electrons and yielded the B_6O-type pattern.

Shearing of a dispersion of this powder in viscous plastic revealed the chainlike agglomerates to be friable and composed of two phases. One phase was a very crystalline B_6X phase and the other phase was BN having strong preferred orientation. Microtomed particles, as shown in Figure 8, revealed B_6X-type particles surrounded by the highly oriented BN. DF microscopy results showed the BN to be oriented along the [001] direction.

The 30% reacted material also consisted of core particles and textured BN. The SAED pattern shown in the micrograph of Figure 9 was typical for this material. The BN texture orientation was parallel to the (001) plane. The BN apparently forms a randomly oriented coat around the core particles with BN growth along the [001] direction. The

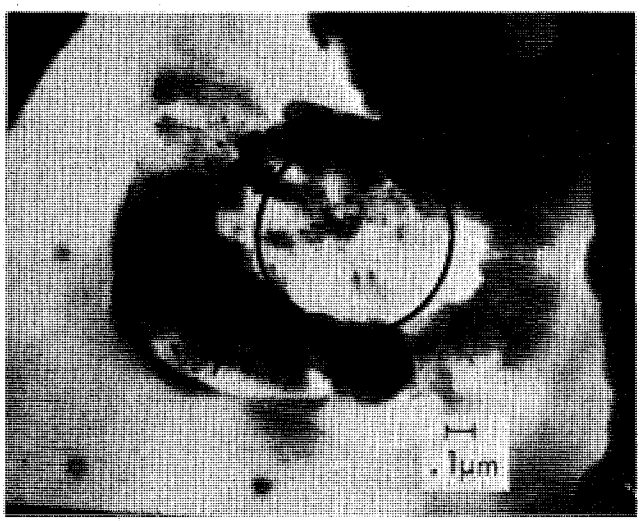

Figure 8. A transmission electron micrograph of a microtomed product chain. SAED pattern indicated the core particle (circled) was B_6X material, whereas, the coating was BN which had grown in the [001] direction.

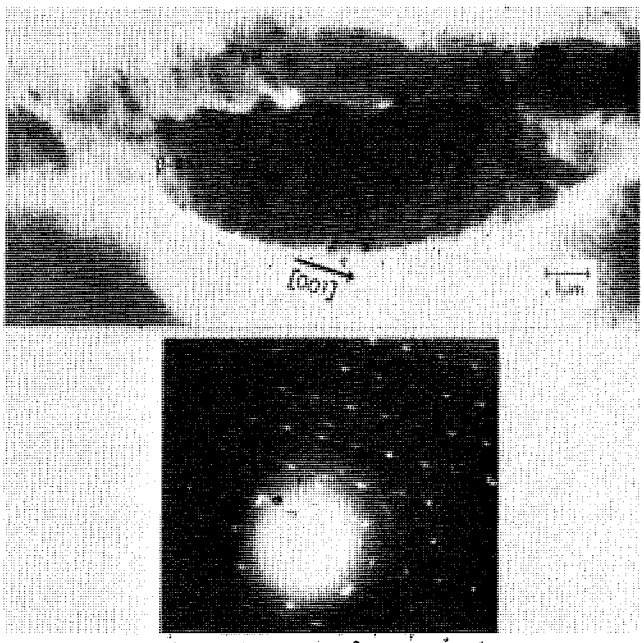

Figure 9. A transmission electron micrograph and a SAED pattern of β-boron particle that has reacted to 30% completion in N_2 (1 atm and 1873 K). The SAED was from the core β-boron particle and shows streaks in the [001] direction. The orientation of this β-boron is the $(\bar{1}10)$ plane. In (111) orientation no streaks are present; therefore, these are rods of intensity indicative of needlelike structures.

patterns from the core particles could be indexed as β-boron except for intensity streaks in the [001] direction. DF electron microscopy showed that the streaks corresponded to sheets of diffracted intensity from needlelike features in the corresponding β-boron crystals. These observations are consistent with the presence of a coherent pre-precipitant phase whose structure is similar to that of β-boron. α-Boron or B_6X material could qualify as candidates for this needlelike structure in the host β-boron.

Discussion

From the rates obtained, the most logical conclusion is that the reaction mechanism is of a mixed nature. The product layer diffusion limited mechanism is eliminated as being very far from a correct fit. The mechanism invoking the outer surface as rate limiting is likewise eliminated since the rate changes during the course of the reaction. Since the rate is weakly dependent on surface area, the most logical mix is the topochemical and reactant phase diffusion. These reactions could be either serial or simultaneous.

Both x-ray analysis and electron diffraction reveal a phase B_6X which, based on oxygen analysis, cannot be completely explained as B_6O. We propose that this phase is actually B_6N (this phase has been suggested by LaPlaca and Post[14]) and may be a metastable form. Furthermore, electron diffraction analysis indicates that under partially reacted conditions a B_6N-type material may be present in the host β-boron, and that under more complete conditions the host material becomes B_6N.

Given this information, the following reactions may be written:

$$\alpha\text{-B} \rightarrow \beta\text{-B} \quad (2)$$

$$6\alpha\text{-B} + \text{N} \rightarrow \text{B}_6\text{N} \quad (3)$$

$$\alpha\text{-B} + \text{N} \rightarrow \text{BN} \quad (4)$$

$$6\beta\text{-B} + \text{N} \rightarrow \text{B}_6\text{N} \quad (5)$$

$$\beta\text{-B} + \text{N} \rightarrow \text{BN} \quad (6)$$

$$\text{B}_6\text{N} + 5\text{N} \rightarrow 6\text{BN} \quad (7)$$

Here N is used to emphasize that some dissociated form of nitrogen is involved in the rate-limiting steps.

Reaction 2 is the inevitable reaction that will occur with any unconverted material. The simultaneous reaction series would involve reactions 3, 4, 5, and 6; whereas, the serial reaction series involves reactions 3, 5, and 7. A modification of the serial mechanism would assume that only α-boron-type material can directly convert to BN. This then assumes reactions 4, 5, and 7, with some sidetracking of α-boron through the reactions 2, 5, and 7. A process of elimination yields the latter mechanism as the logical choice. The next three paragraphs summarize the logic used to eliminate the first two mechanisms.

Proper assumptions about the reaction velocities would allow the simultaneous series. One could assume the average overall velocity of reaction 3 to be slow compared to reaction 4 ($\bar{\nu}_3 \ll \bar{\nu}_4$) to account for the observation of little or no B_6N when amorphous boron (α-B) reacts with N_2. The presence of B_6N and BN for the reaction with β-boron would imply that the average velocities of reactions 5 and 6 would be nearly equal ($\bar{\nu}_5 \approx \bar{\nu}_6$).

To explain why the topochemical reaction by α-boron is slower than expected, the remaining assumption that the velocity of reaction 4 is less than reaction 6 ($\bar{\nu}_4 < \bar{\nu}_6$) presents no conflict. However, one would expect B_6N to be found uniformly distributed through the β-boron and BN formed from β-boron since reaction 5 is homogeneous. The cores of B_6N observed by electron microscopy and SAED indicate this is incorrect. Therefore, the presence of reaction 7 must be invoked.

The serial reaction series using reactions 3, 5, and 7 has a conflict between reaction velocities. Since the reaction product of α-boron with nitrogen is void of B_6N, one must conclude that reaction 7 is more rapid than reaction 3 ($\bar{\nu}_7 \gg \bar{\nu}_3$). This means that the rate-limiting step in the overall process from α-boron to BN is reaction 3 and is purely the reactant phase diffusion mechanism. This would imply that the overall conversion of α-boron to BN would be slower than the conversion of β-boron which is not the case because the average velocity of reaction 5 must be equal to or greater than reaction 7 ($\bar{\nu}_5 \geq \bar{\nu}_7$) to observe the B_6N.

The remaining mechanism (which assumes BN can form only from either α-boron or B_6N) presents no conflicts with the experimental data. The reaction velocities are such that reaction 4 is slower than reaction 7, and reaction 5 is equal to or greater than reaction 7 ($\bar{\nu}_4 < \bar{\nu}_7 \leq \bar{\nu}_5$). This explains why the linear rate constant for the topochemical reaction with α-boron is about 200–400 times slower than for β-boron conversion. Furthermore, since the direct conversion of α-boron to B_6N is not allowed, the B_6N must be formed from α-boron by the indirect series of reactions 2 and 5. This explains the small amount or lack of B_6N in the reactions with α-boron. Utilization of reactions 5 and 7 allows the observation of cores of B_6N in the 60% complete reaction and cores of β-boron with B_6N in the 30% complete reaction.

Conclusion

As a result of this study, it is concluded that the reaction of boron with nitrogen involves both topochemical and reactant phase diffusion mechanisms. The reactions involved are:

$$\alpha\text{-B} + \text{N} \rightarrow \text{BN} \quad (8)$$

which is topochemical, and

$$6\beta\text{-B} + \text{N} \rightarrow \text{B}_6\text{N} \quad (9)$$

which utilizes the reactant phase diffusion–nucleation mechanism, and

$$\text{B}_6\text{N} + 5\text{N} \rightarrow 6\text{BN} \quad (10)$$

which is topochemical. The other minor reaction that occurs is:

$$\alpha\text{-B} \rightarrow \beta\text{-B} \qquad (11)$$

Acknowledgment. Work performed under Contract W-7405-eng-26 with the United States Energy Research and Development Administration.

Appendix

For a weight distribution of particles with respect to radius, $F_\omega(r)$, the overall weight gain curves for the topochemical and diffusion controlled mechanisms can be derived. For the topochemical mechanism

$$dx/dt = -k \qquad (A)$$

where x is the instantaneous distance from the center to the reaction front. For the diffusion controlled mechanism

$$dx/dt = -k/(r-x) \qquad (B)$$

The integrated forms of A and B are

$$r - x = kt \text{ for A} \qquad (C)$$

and

$$r - x = \sqrt{2kt} \text{ for B} \qquad (D)$$

A parameter τ will be used for both cases to replace kt for eq C and $(2kt)^{1/2}$ for eq D. It will be noted that eq C and D are valid only if $r \geq \tau$.

$$r - x = \tau \qquad r \geq \tau \qquad (E)$$

$$r = 0 \qquad r \leq \tau \qquad (F)$$

The ratio of the weight gain of a particular partial radius at any time, $\omega(t,r)$, to the final weight gain, $\omega(\infty,r)$ is given by

$$\omega(t,r)/\omega(\infty,r) = (r^3 - x^3)/r^3 \qquad (G)$$

for a solid or

$$\frac{\omega(t,r)}{\omega(\infty,r)} = \frac{3\tau}{r} - \frac{3\tau^2}{r^2} + \frac{\tau^3}{r^3} \qquad \text{for } r \geq \tau \qquad (H)$$

$$\frac{\omega(t,r)}{\omega(\infty,r)} = 1 \qquad \text{for } r \leq \tau \qquad (I)$$

Thus for total weight gain $\omega_T(t)$ for all the particles one has

$$\frac{\omega_T(t)}{\omega_T(\infty)} = F_\omega(\tau) + \int_{r=\tau}^{r_{max}} \frac{\partial F_\omega(r)}{\partial r}\left(\frac{3\tau}{r} - \frac{3\tau^2}{r^2} + \frac{\tau^3}{r^3}\right) dr \qquad (J)$$

In practice $F_\omega(r)$ was measured at a finite number of radii and could thus be approximated by straight lines between measurements. Therefore, let

$$C_i = \frac{\partial F_\omega(r_{i-1} \text{ (or) } \tau < r \leq r_i)}{\partial r} \qquad (K)$$

and eq J may be integrated to give

$$\frac{\omega_T(\tau)}{\omega_T(\infty)} = F_\omega(r_j) + (\tau - r_j)C_j + \sum_{i=j+1} C_i\left[3\tau \ln \frac{r_i}{\max(r_{i-1},\tau)} + 3\tau^2\left(\frac{1}{r_i} - \frac{1}{\max(r_{i-1},\tau)}\right) - \frac{\tau^3}{2}\left(\frac{1}{r_i^2} - \frac{1}{(\max(r_{i-1},\tau))^2}\right)\right] \qquad (L)$$

where r_j is the highest value bounded by τ ($r_j = r_{i,max} \leq \tau$).

Registry No. BN, 10043-11-5; B_6N, 59765-75-2; N_2, 7727-37-9; B, 7440-42-8.

References and Notes

(1) J. B. Condon and E. A. Larson, *J. Chem. Phys.*, **59**, 855 (1973).
(2) F. N. Rhines, *Trans. Am. Inst. Min., Metall. Pet. Eng.*, 246 (1940); *J. Corrosion*, **4**, 15 (1947).
(3) F. N. Rhines, W. A. Johnson, and W. A. Anderson, *Trans. Am. Inst. Min., Metall. Pet. Eng., Tech. Publ.*, **No. 1368** (1941).
(4) J. B. Condon, "Calculations of Nonspalling Isothermal Hydriding Rates for Uranium", Y-1963, Union Carbide Corporation, Nuclear Division, Oak Ridge Y-12 Plant, Oak Ridge, Tenn., Oct. 1974.
(5) K. Niedenzer and J. W. Dawson, "Boron-Nitrogen Compounds", Academic Press, New York, N.Y., 1965.
(6) V. M. Sleptsov and G. V. Samsonov, *Dopov. Akad. Nauk. Ukr. R.S.R.*, 1116–18 (1959).
(7) H. F. Rizzo, W. C. Simmons, and H. O. Bielstein, *J. Electrochem. Soc.*, **109**, 10795 (1962).
(8) D. R. Petrak and R. Ruh, *Natl. Bur. Stand. (U.S.), Spec. Publ.*, **No. 364**, 605 (1972).
(9) G. V. Samsonov, L. Ya Markovskii, A. F. Zhigaeh, and M. G. Valyashko, "Boron—Its Compounds and Alloys", Publishing House of the Academy of Science of the Ukraninian S.S.R., Kiev, 1960. Available in translation AEC-tr-5032. See p 51.
(10) A. E. Newkirk, *Adv. Chem. Ser.*, **No. 32**, 27–41 (1961).
(11) J. L. Hoard and R. E. Hughes, "The Chemistry of Boron and Its Compounds", E. L. Muetterties, Ed., Wiley, New York, N.Y., 1967, pp 25–154.
(12) C. E. Holcombe, Jr., and O. J. Horne, Jr., *J. Am. Ceram. Soc.*, **55**, 106 (1972).
(13) P. Runow, *J. Mater. Sci.*, **7**, 499–511 (1972).
(14) S. LaPlaca and B. Post, *Planseeber. Pubvermetall.*, **9**, 109 (1961).

Contribution from the Chemistry Division,
Oak Ridge National Laboratory, Oak Ridge, Tennessee 37830

Identification of Polyborate and Fluoropolyborate Ions in Solution by Raman Spectroscopy

L. MAYA

Received March 8, 1976 AIC60182F

The polymeric ions $B_5O_6(OH)_4^-$, $B_3O_3(OH)_4^-$, $B_4O_5(OH)_4^{2-}$, and $B_3O_3F_6^{3-}$ have been identified in solution and their regions of stability established. Comparisons of Raman spectra of the solutions with the spectra of solid reference materials containing the same structural entities, $NaB_5O_8 \cdot 5H_2O$, orthorhombic metaboric acid $(HBO_2)_3$, $Na_2B_4O_7 \cdot 10H_2O$, and $Na_3B_3F_6O_3$ were used to identify the ions. The charge on the polyborate ions was established on the basis of material and ionic balances. The hydrolytic behavior of $Na_3B_3F_6O_3$ was established. This compound is partially depolymerized into $BF_2(OH)_2^-$ ions which disproportionate into BF_3OH^-, F^-, and H_3BO_3. A new synthesis for $Na_3B_3F_6O_3$ was developed.

Introduction

The presence of polyborate ions in solution has been established by cryoscopic methods, nuclear magnetic resonance, ir, conductance, pH titration, and temperature jump techniques. These studies have shown that equilibrium between polyborate species is very fast and changes in equilibrium compositions do not take place. The most extensive work on the subject is that of Ingri[1,2] who postulated, on the basis of